Journal of Solid State Chemistry **165,** 375–380 (2002)
doi:10.1006/jssc.2002.9555, available online at http://www.idealibrary.com on IDEAL®

Effect of Quenching on Magnetoresistance Properties in the $Pr_{0.5}Sr_{0.5}MnO_3$ Perovskite Manganite

W. Boujelben,* M. Ellouze,* A. Cheikh-Rouhou,*,[1] J. Pierre,† and J. C. Joubert‡

*Laboratoire de Physique des Matériaux, Faculté des Sciences de Sfax, B. P. 802, 3018 Sfax, Tunisie; †Laboratoire Louis NEEL, CNRS, B. P. 166X, 38042 Grenoble, France; and ‡Laboratoire des Matériaux et du Génie Physique, ENSPG-CNRS (UMR-5628), B. P. 46, 38402 Saint Martin d'Hères Cedex, France

Received October 8, 2001; in revised form January 25, 2002; accepted February 22, 2002

We report on the magnetization, resistivity and magnetoresistance (MR) measurements on polycrystalline $Pr_{0.5}Sr_{0.5}MnO_3$. Quenching samples from 1400°C to room temperature in water (sample I) or in air (sample II) leads to different behaviors. Powder X-ray diffraction patterns for samples I and II could be indexed, respectively, in rhombohedral perovskite structure with $R\bar{3}c$ space group and in the orthorhombic one with *Imma* space group. Magnetization measurements show that both samples exhibit a paramagnetic–ferromagnetic transition at 280 K (sample I) and 265 K (sample II). At low temperature, sample I presents a ferromagnetic spin-canted state, while sample II behaves as an antiferromagnet below 160 K. Resistivity and magnetoresistance studies show a net difference as a function of the quenching conditions. © 2002 Elsevier Science (USA)

Key Words: **manganites; perovskite; resistivity; magnetoresistance; quenching effect.**

1. INTRODUCTION

With the discovery of the very large negative magnetoresistance, a considerable interest has been focused on the perovskite-type hole doped manganese oxides (1–7). Such oxides with general formula $Ln_{1-x}A_xMnO_3$, where Ln is a trivalent rare-earth element and A is a divalent alkali-earth one, exhibit an insulator–metal transition for $0.2 < x < 0.5$ which occurs near their Curie temperature T_C. Previous magnetic studies showed that $Pr_{0.5}Sr_{0.5}MnO_3$ exhibits two transitions versus temperature, from paramagnetic (PM) state to ferromagnetic (FM) one at $T_C = 265$ K and from FM to an antiferromagnetic (AFM) and charge-ordered (CO) or orbital-ordered state at about 140 K (8–10). However, other studies showed that the PM–FM transition was followed by a decrease of the magnetization indicating an FM spin-canted state (11). In order to study the effect of quenching on the electrical and magneto-transport properties of this sample, we have carried out magnetic and electrical measurements on two $Pr_{0.5}Sr_{0.5}MnO_3$ samples, one quenched in water and the other in air from 1400°C to room temperature.

2. EXPERIMENTAL

Powder samples of $Pr_{0.5}Sr_{0.5}MnO_3$ were prepared by mixing Pr_6O_{11}, Mn_2O_3 and $SrCO_3$ up to 99.9% purity in the desired proportion according to the reaction

$$0.5Pr_6O_{11} + 3SrCO_3 + 3Mn_2O_3 \rightarrow 6Pr_{0.5}Sr_{0.5}MnO_3 + \delta\ CO_2.$$

The starting materials were intimately mixed in an agate mortar and then heated in air at 1000°C for 60 h. A systematic annealing at high temperature is necessary to ensure a complete reaction. In fact, the powders are pressed into pellets (of about 1 mm thickness) and sintered at 1400°C in air for 60 h with intermediate regrinding. Finally, the pellets were rapidly quenched to room temperature in air or in water (pellet inside the platinum crucible in water) without contact between water and the pellet.

Phase purity, homogeneity, and cell dimensions were determined by powder X-ray diffraction at room temperature [Guinier-Hagg cameras with Cr$K\alpha$ radiation for the sample quenched in water (sample I) and diffractometer with Cu radiation for the sample quenched in air (sample II) and Si powder as internal standard]. Unit-cell dimensions were obtained by least-squares calculations.

The magnetization measurements versus temperature with several magnetic applied fields up to 8 T were recorded by a vibrating sample magnetometer in the temperature range 4.2–350 K.

Resistivity measurements as a function of the temperature and the applied magnetic field were carried out on dense ceramic pellets by the standard four-probe technique.

[1] To whom correspondence should be addressed. Fax: + 216-74-274437. E-mail: abdel.cheikhrouhou@fss.mu.tn.

0022-4596/02 $35.00

3. RESULTS AND DISCUSSION

3.1. X-Ray Diffraction Analysis

X-ray diffraction patterns at room temperature of both samples are shown in Fig. 1. Our samples are single phase and have a perovskite structure. Sample I crystallizes in rhombohedral structure with $R\bar{3}c$ space group (11); however, sample II crystallizes in the orthorhombic symmetry with *Imma* space group. This result has also been observed by Rao *et al.* (12) and Wolfman *et al.* (13).

In Table 1 we list the crystallographic data for both samples.

TABLE 1
Crystallographic Data for Both $Pr_{0.5}Sr_{0.5}MnO_3$ Samples Quenched in Water and in Air

	Space group	a (Å)	b (Å)	c (Å)	a_r (Å)	α_r (°)	V (Å^3)
Sample I	$R\bar{3}c$	—	—	—	5.441	60.333	229.710
Sample II	*Imma*	5.3971	5.3988	7.7748	—	—	226.543

3.2. Magnetic Properties

In Fig. 2 we have plotted magnetization as a function of temperature with an applied field of 500 Oe. Samples I and II exhibit a PM–FM transition at 280 and 265 K, respectively. This PM–FM transition is followed by an FM–AFM (antiferromagnetic) one at 160 K for sample II and by a decrease of the magnetization for sample I which may indicate a spin-canted state at low temperature. The AFM state observed in sample II is in concordance with previous work on powder sample in an applied field of 0.01 T (10, 14). The transition temperatures (PM–FM and FM–AFM) are found to be 260 and 150 K, respectively. The difference in the transition temperature values may be attributed to the elaborating method.

A magnetization evolution versus temperature as in sample I has been previously observed only on epitaxial $Pr_{0.5}Sr_{0.5}MnO_3$ thin film (15) with a T_C of 263 K.

In order to confirm this different behavior at low temperatures, we have carried out magnetization measurements as a function of applied magnetic field up to 8 T at several temperatures below T_C. These measurements have been plotted in Fig. 3. Our results confirm the PM–FM transition with spin-canted state at low temperatures for

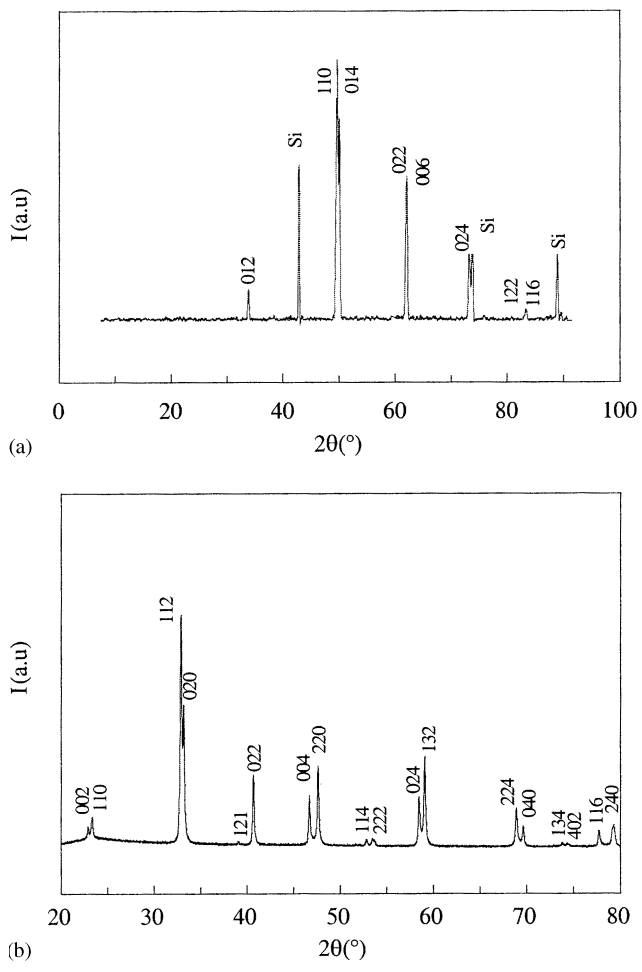

FIG. 1. X-ray diffraction patterns for both samples: (a) sample I and (b) sample II.

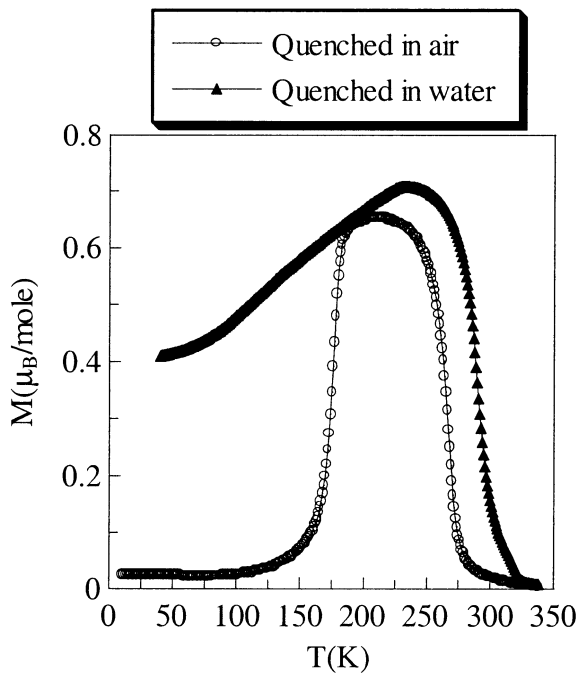

FIG. 2. Evolution of magnetization as a function of temperature at $H = 0.05$ T for both samples.

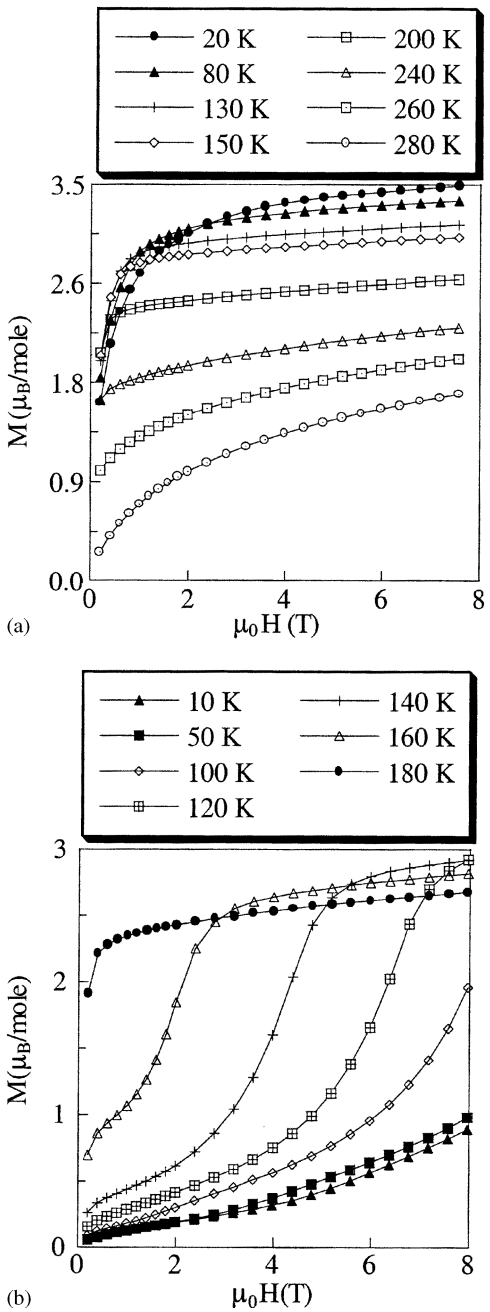

FIG. 3. Magnetization evolution versus applied magnetic field for several temperatures for both samples: (a) sample I and (b) sample II.

sample I (Fig. 3a) and the FM–AFM transition in the range $160\ \mathrm{K} < T_N < 180\ \mathrm{K}$ for sample II (Fig. 3b). The AFM behavior becomes more clear with decreasing temperature. Two phases, one ferromagnetic, the other metamagnetic, seem to coexist in the range 120–170 K. The energy difference between the two phases decreases with temperature and may be obtained roughly by $M_F \times H_C$ (M_F is the magnetization of the ferromagnetic phase, and H_C is the critical field of the metamagnetic one).

We have reported more details on the magnetic behavior of our two samples and the quenching effect on these properties elsewhere (16).

3.3. *Electrical Properties*

The resistivity measurements as a function of temperature in zero field and in the temperature range 4.2–300 K in cooling mode are shown in Fig. 4 for both samples. As we can observe, the electrical properties are substantially different. These results underline the effect of quenching method on these properties.

Using the sign of the resistivity $d\rho/dT$ as a criterion, we found that sample I exhibits three electrical behaviors as

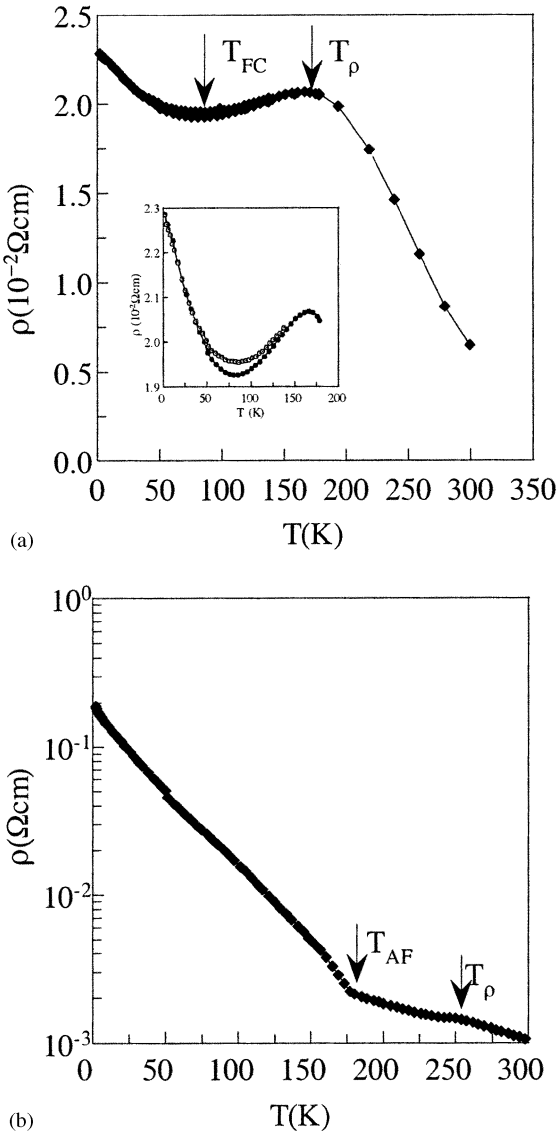

FIG. 4. The resistivity evolution as a function of temperature at $H = 0$ T for both samples: (a) sample I and (b) sample II.

a function of temperature: a semiconductor behavior above $T_\rho \approx 200$ K followed by a metallic-like one in the temperature range $T_{FC} \leq T \leq T_\rho$ and finally a semiconducting one below T_{FC}. T_{FC} is found to be 86 K. This sample is ferromagnetic between T_{FC} and T_ρ and becomes canted ferromagnetic-semiconducting below T_{FC}. This semiconducting behavior at low temperature can be explained by the spin-canted state which leads to a difficult charge transfer between neighboring sites according to the double-exchange theory. For sample I we also observe that the zero-field resistivity $\rho(T)$ reveals a thermal hysteresis in the temperature range 50–150 K between the cooling and warming-up modes. In the paramagnetic phase, the resistivity measurements can be fitted by a thermally activated conduction indicating hopping polaron conduction $\rho = (kT/ne^2D)\exp(E_{hopp}/kT)$ where eD/kT is the Einstein diffusion mobility, n the carrier density, D the diffusion constant and E_{hopp} the hopping energy. The hopping energy is found to be 0.09 eV. In the range between T_{FC} and T_ρ, the long-range ferromagnetic order suppresses magnetic polarons, and promotes the carrier hopping, which becomes again hindered when the canted structure occurs.

For sample II, our resistivity measurements show a semiconducting behavior in the whole temperature range with three different evolutions, above T_ρ, for $T_{AF} < T < T_\rho$ and below T_{AF}. The difference between the resistivity values at low and room temperatures is quite high compared to that obtained in sample I. In fact, the ratio of low temperature to room temperature resistivity values is found to be 2×10^2 and 5 for samples II and I, respectively, but on the contrary, ρ at room temperature is 7 times higher for sample I. We have fitted our resistivity data for $T_{AF} < T < T_\rho$ and for $T > T_\rho$ by the above law. The hopping energy is found to be 39.6 and 70.1 meV for $T_{AF} < T < T_F$ and $T > T_\rho$, respectively. All these values are less than those obtained for sample I. Although the polaron law seems to fit the data, correctly another suitable law may be the Mott law $\rho = \rho_0(T_0/T)^{1/4}$ related to localization phenomena. $T_0^{1/4}$ is found to be 18.2 and 31.5 $K^{1/4}$ for $T_{AF} < T < T_\rho$ and for $T > T_\rho$, respectively. Due to the restricted ranges of temperatures investigated, we are not able to decide for one or the other law. Within the framework of localization, we will say that for sample II, the localization is largest in the paramagnetic range due to the magnetic disorder, it decreases below T_C due to the onset of ferromagnetic state, leading to a band splitting and to the reduction of localization energy for one of the spin subbands. Nevertheless, the magnetic splitting is not enough to bring the Fermi level below the mobility edge for that subband; thus, we do not reach a metallic-like regime. Below T_{AF}, the antiferromagnetic and charge-ordered state restores a semiconducting- like resistivity. The stronger amplitude of the resistivity variations is due to a much better charge- or orbital-ordered state, probably linked to a better chemical order.

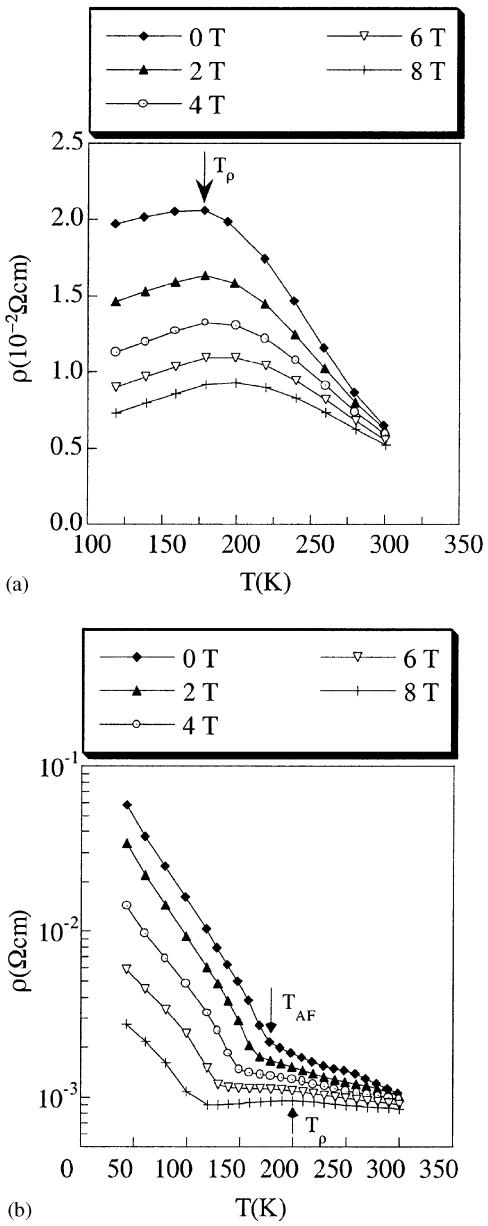

FIG. 5. The resistivity evolution as a function of temperature at several applied fields for both samples: (a) sample I and (b) sample II.

In order to study the effect of the magnetic applied field on the transport properties, we have carried out resistivity measurements as a function of temperature in several magnetic fields up to 8 T in cooling mode. Our measurements have been performed for sample II in the temperature range 50–300 K and only in the temperature range 120–300 K for sample I. Our data have been plotted in Fig. 5. For sample I, we observe a semiconductor–metal transition when the temperature decreases, the same behavior as in zero applied field. For sample II, a semiconducting behavior in the whole temperature range is obtained. However, for $H \geq 6$ T, a metallic-like behavior seems to appear below T_ρ; in fact, in

TABLE 2
Hopping Energy Data for Sample Quenched in Water in the Paramagnetic Phase

H (T)	E_{hopp} (meV)
0	91.1
2	80.7
4	72.6
6	65.8
8	60.0

the temperature range $T_{AF} < T < T_\rho$, there seems to be a competition between a semiconducting and metallic-like behavior. The metallic behavior overcomes the semiconducting one when the applied field increases above 8 T.

The magnetic field induces a decrease in the maximum resistivity value and an increase in the transition temperature. Our data in the paramagnetic phase have been fitted by the same law as above. The hopping energy decreases with increasing magnetic field. In Table 2 we list the hopping energy values.

On the other hand, for sample II, a semiconducting behavior remains in the whole temperature range; this semiconducting behavior is characterized by three regions. The magnetic applied field induces a decrease in the resistivity values and the T_{AF} shifts to lower values, which has been explained previously through the energy difference between the ferromagnetic and antiferromagnetic phases. Our data for $T_{AF} < T < T_\rho$ and for $T > T_\rho$ in a magnetic applied field up to 6 T and for $T > T_\rho$ at 8 T have been fitted using the above law. In Table 3 we list the hopping energy values.

The hopping energy E_{hopp} in both temperature ranges decreases with increasing magnetic applied field. Both laws indicated above cannot fit our resistivity data for $T < T_{AF}$ because our sample exhibits an antiferromagnetic behavior in this temperature range.

The magnetoresistance evolution versus temperature at several applied magnetic fields is illustrated in Fig. 6. The magnetoresistance, defined as $(\rho(H)\text{-}\rho(0))/\rho(0)$, increases with increasing applied magnetic field and with decreasing temperature for both samples. It is found to be 60 and 95% at low temperature and at 8 T for samples I and II, respectively.

TABLE 3
Hopping Energy Data for Sample Quenched in Air for $T_{AF} < T < T_\rho$ and $T > T_\rho$

H (T)	T_{AF} (K)	T_ρ (K)	E_{hopp} (meV) $T_{AF} < T < T_\rho$	E_{hopp} (meV) $T > T_\rho$
0	180	260	39.6	70.1
2	170	230	32.1	44.7
4	150	220	23.9	37.5
6	130	210	16.5	32.7
8	120	200	—	27.2

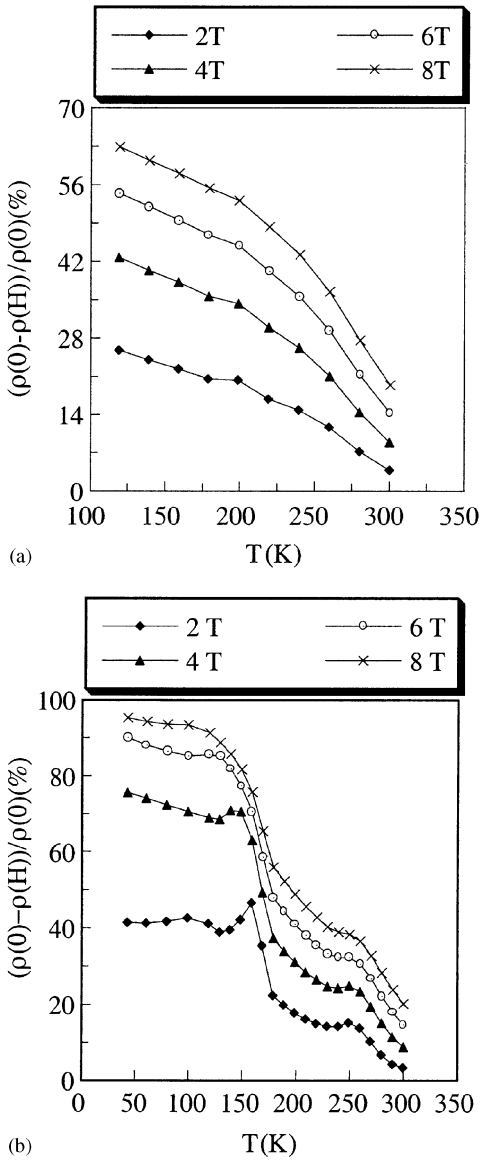

FIG. 6. Magnetoresistance evolution as a function of temperature for both samples: (a) sample I and (b) sample II.

We thus obtain large, if not colossal, magnetoresistance effects on both systems. In the case of air-quenched sample II, the resistivity below T_C strongly decreases under field and an intermediate nearly metallic-like regime is obtained above 6 T. In fact, we may have a coexistence of ferromagnetic and AF regions. For annealed samples, it should probably turn metallic. The transition temperature T_{AF} strongly decreases, as the application of field melts the zero-field AF-CO state; the resistivity also strongly drops following the canting angle or the proportion of ferromagnetic phase; therefore, it is difficult to explain this effect in

terms of canting angle, or in terms of percolation through ferromagnetic-ordered regions (17–20).

Coming back to sample I (quenched in water), the shapes of the resistivity and MR curves versus temperature recall in some way those found in granular materials. In this last case, the scattering at grain boundaries is much larger than that in grains themselves, the resistivity shows a maximum well below the Curie point, and the intrinsic resistivity peak at T_C is often not visible, which is the case for sample I. We may also note that the room temperature resistivity is 7 times larger than that for the air-quenched sample II. One reason for the present behavior may probably be found in the small grain structure of the water-quenched sample (the crystallite size is about 2 μm for sample I and 4 μm for sample II). The large MR observed below 200 K is for one part due to melting of the incomplete AF charge-order state, but may be due for another part to the contribution of grain boundaries which remains significant down to low temperatures (21).

4. CONCLUSION

We have investigated the effect of quenching on the magneto-transport properties of polycrystalline $Pr_{0.5}Sr_{0.5}MnO_3$ sample. Our studies show that these properties strongly depend on the quenching conditions. While the sample quenched in water presents a broad semiconducting–metallic transition well below T_C followed by a semiconductor behavior at low temperatures, the sample quenched in air shows well-defined regimes in resistivity and MR. Both exhibit, at low temperature and for an applied field of 8 T, colossal magnetoresistance effects of 60 and 95% for samples I and II, respectively.

ACKNOWLEDGMENTS

This study has been supported by the Tunisian Ministry of Scientific Research and Technology.

REFERENCES

1. R. Von Helmolt, J. Wecker, B. Holzapfel, L. Schutz, and K. Samwer, *Phys. Rev. Lett*. **71,** 2331 (1993).
2. K. Chahara, T. Ohno, M. Kassai, and Y. Kosono, *Appl. Phys. Lett*. **63,** 1990 (1993).
3. R. D. Sanchez, J. Rivas, C. V. Vazquez, A. L. Quintela, M. T. Causa, M. Tovar, and S. Oseroff, *Appl. Phys. Lett*. **68,** 134 (1996).
4. H. L. Ju and H. Sohn, *J. Magn. Magn. Mater*. **167,** 200 (1997).
5. C. N. R. Rao and B. Raveau, Eds., in "Colossal Magnetoresistance, Charge Ordering and Related Properties of Manganese Oxides," World Scientific, Singapore, 1998.
6. A. Peles, H. P. Kunkel, X. Z. Zhou, and Gwyn Williams, *J. Phys.: Condens. Matter* **11,** 8111 (1999).
7. W. Boujelben, A. Cheikh-Rouhou, M. Ellouze, and J. C. Joubert, *Phys. Stat. Sol. A* **177,** 503 (2000).
8. Y. Tomioka, A. Asamitsu, Y. Moritomo, H. Kuwahara, and Y. Tokura, *Phys. Rev. Lett*. **74,** 56 (1995).
9. H. Kawano, R. Kajimoto, H. Yoshizawa, Y. Tomioka, H. Kuwahara, and Y. Tokura, *Phys. Rev. Lett*. **78,** 4253 (1997).
10. C. Martin, A. Maignan, M. Hervieu, and B. Raveau, *Phys. Rev. B* **60,** 12191 (1999).
11. W. Boujelben, A. Cheikh-Rouhou, M. Ellouze, and J. C. Joubert, *Phase Transitions* **71,** 127 (2000).
12. C. N. R. Rao, P. N. Santhosh, R. S. Singh, and A. Arulraj, *J. Solid State Chem.* **135,** 169 (1998).
13. J. Wolfman, C. H. Simon, M. Hervieu, A. Maignan, and B. Raveau, *J. Solid State Chem.* **123,** 413 (1996).
14. C. Martin, A. Maignan, F. Damay, M. Hervieu, B. Raveau, Z. Jirak, G. André, and F. Bourée, *J. Magn. Magn. Mater*. **202,** 11 (1999).
15. P. Wagner, V. Metlushko, M. Van Bael, R. J. M. Vullers, L. Trappeniers, A. Vantomme, J. Vanacken, G. Kido, V. V. Moshchalkov, and Y. Bruynseraede. *J. Phys. IV* **6,** C3-309 (1999).
16. W. Boujelben, A. Cheikh-Rouhou, J. Pierre, and J. C. Joubert, *J. Alloys Compd*. **314,** 15 (2001).
17. A. Anane, C. Dupas, K. Le Dang, J. P. Renard, P. Veillet, A. M. De Léon-Guevara, P. Berthet, F. Millot, and A. Revcolevschi, *Phys. Rev. B* **56,** 6031 (1997).
18. A. Moreo, S. Yunoki, and E. Dagotto, *Science* **283,** 2034 (1999).
19. M. Uehara, S. Mori, C. H. Chen, and S.-W. Cheong, *Nature* **399,** 560 (1999).
20. M. Yu. Kagan, D. I. Khomskii, and M. V. Mostovoy, *Eur. Phys. J. B* **12,** 217 (1999).
21. H. Y. Hwang, S. W. Cheong, P. G. Radaelli, M. Marezio, and B. Batlogg, *Phys. Rev. Lett*. **72,** 2636 (1994).